minerals

MDPI

Article

Exploring Smoothing and Interpolation in Thellier-Type Paleointensity Determinations

Lluís Casas [1,*], Marc Ortiz [2] and Roberta Di Febo [1]

[1] Departament de Geologia, Universitat Autònoma de Barcelona (UAB), Edifici C, 08193 Cerdanyola del Vallès, Catalonia, Spain; roberta.difebo@uab.cat
[2] Geo-Min, Carrer Noguera, 6, 43151 Tarragona, Catalonia, Spain; mao.r.mo@hotmail.com
* Correspondence: lluis.casas@uab.cat

Abstract

Smoothing and interpolation of zero-field (Z) and infield (I) heating steps in Thellier-type paleointensity determinations have been tested. Paleomagnetic samples of different materials were artificially magnetized with an applied field of 50 μT. Six samples were measured following the standard double-heating Coe-variation experimental protocol, and the obtained results were used to test several mathematical functions to smooth the experimental data. The best smoothed results were obtained using a Five Parameters Logistic (5PL) function that resulted in field estimates of good quality, although not better than those obtained experimentally. Therefore, the smoothing of de- and remagnetization data appears unnecessary. In addition to smoothing, the tested functions can be used to interpolate additional Z and, indirectly, also I steps. Interpolation using cubic Hermite splines (without any smoothing) displays a better performance than interpolation (and smoothing) using the 5PL function. A new single-step heating method is presented, combining experimental and interpolated de- and remagnetization steps. The new method would not be applicable for retrieving reliable ancient field intensities on its own, but it could save measuring time under some circumstances.

Keywords: paleomagnetic intensity; Thellier; smoothing; interpolation; single-step

Academic Editor: Michael S. Zhdanov

Received: 17 June 2025
Revised: 6 August 2025
Accepted: 17 August 2025
Published: 19 August 2025

Citation: Casas, L.; Ortiz, M.; Di Febo, R. Exploring Smoothing and Interpolation in Thellier-Type Paleointensity Determinations. *Minerals* **2025**, *15*, 873. https://doi.org/10.3390/min15080873

1. Introduction

The estimation of the geomagnetic field intensity of the past constitutes a branch of paleomagnetism usually referred to as paleointensity determinations. These determinations can be achieved from samples carrying a natural thermoremanent magnetization (NRM), such as volcanic rocks and baked clays. The most common remanence carriers are magnetically ordered minerals like magnetite, often also including members of the titanomagnetite solid solution series, ($Fe_{3-x}Ti_xO_4$), hematite (α-Fe_2O_3) and, to a less extent, maghemite (γ-Fe_2O_3).

Paleointensity determinations help to reconstruct the strength of the Earth's part magnetic field, and they are often used for dating purposes. A common method to extract paleointensities from samples is the Thellier experiment [1] and its variations. The method relies on several general properties of thermoremanent magnetizations known as Thellier laws [2], which hold for noninteracting single domain (SD) magnetic carriers. Under certain circumstances, it is assumed that the NRM and the ancient field (B_{anc}) have a linear proportionality that can be described simply using a scalar (A) instead of a tensor [3]:

$$NRM = A \cdot B_{anc}$$

Moreover, it is assumed that this scalar remains unchanged, and thus it is the same constant value that relates a magnetic field imparted to the sample at the laboratory with the corresponding artificial thermoremanent magnetization (TRM):

$$TRM = \mathrm{A} \cdot B_{lab}$$

Then, the generalized absolute paleointensity estimate of the ancient field (B_{anc}) from a laboratory measurement can be summarized as [4]

$$B_{anc} = \frac{NRM}{TRM} \cdot B_{lab} \quad (1)$$

However, paleointensity determinations are a bit more complex. Factors such as magnetic overprints, chemical alteration, remanence sources other than thermoremanence, and magnetic interactions between neighboring magnetic particles can result in wrong estimations of the paleomagnetic field. Therefore, typically, the remanences (NRM and TRM) are not measured in single steps but in a series of double-heating steps, progressively increasing the heating temperature. The most common experimental protocols mix double-heating steps, often combining zero-field (Z) and infield (I) steps [3], and possibly the most commonly applied protocol is the so-called Coe variation [5], for which the heating sequence is "ZI". In each double-heating (and cooling) step, a portion of the NRM is demagnetized and a partial thermoremanence (pTRM) is acquired in the infield step. Using the demagnetization steps, it is possible to plot a Zijderveld diagram [6], as is routinely done in paleomagnetic direction estimations. This is useful to detect magnetic overprints, and a reliable paleodirection could be obtained if the sample was obtained in situ and its orientation marked during sampling. Combining both zero- and infield steps, it is possible to plot an Arai diagram [7], which is a plot of newly acquired pTRM versus the remaining NRM (rNRM), both normalized to the initial NRM value. For a Thellier-type experiment considered to be successful, the Arai plot will show a straight line, and its slope multiplied by $|B_{lab}|$ is the overall paleointensity estimate. However, the estimate is usually corrected to account for anisotropy of the remanence [4,8] and different rates of cooling [9,10]. Anisotropy corrections are particularly important for archaeological materials (e.g., baked clays with strong fabric) and require the determination of the TRM anisotropy tensor. Cooling rate corrections are needed for samples that cooled slowly (over hours to days), like those from lava flows, baked clays, or burned soil. Uncorrected measurements would lead to overestimated paleomagnetic field intensities.

Furthermore, the remanence carriers are often not strictly SD particles; usually, they are pseudo-single domain (PSD) particles [11], and as their sizes increase, they tend toward the multidomain (MD) regime, and the Thellier laws are violated. In this situation, the Arai diagrams tend to lose linearity, typically exhibiting concave-up shapes [12] and other non-ideal (i.e., non-linear) shapes [13]. A number of experimental protocols of Thellier-type experiments have been designed to detect non-ideal behavior [14], including additional steps like "pTRM checks" [15] to detect alteration or "pTRM tail checks" to identify MD behavior [16]. The nature of the remanence assemblage (SD, PSD, or MD) can even affect the TRM intensity dependence with cooling rate [10], and SD assemblies are particularly sensitive to the cooling rate effect [9].

The whole process (remanence measurements and heating steps) is tedious, particularly when the heating steps reach high temperatures. The heating steps are time-consuming because the samples are kept at high temperature for at least one hour, and, if cooling is not fan-assisted, cooling ramps can take a similar amount of time, even when applying a cooling rate much higher than the one that created the original NRM. To optimize the time, a battery of samples is heated in every step. One disadvantage of collectively heating the

samples is that any technical or operational problem will affect the whole set of samples. Another issue arises when the heated set has different blocking temperature spectra because a given series of heating steps could be convenient for some samples but not for others.

Some accidents can easily occur in a series of measurements, for instance, a malfunction of the oven during a heating step, a temperature setting mistake, or an unintentionally skipped heating step. In such cases, the normal procedure is to delete the corresponding "ZI" double step. However, another possibility would be to interpolate the missing steps. Some mathematical functions can be used to simulate the de- and remagnetization curves; these can be used to interpolate heating steps and also to smooth the experimental data.

In this paper, we investigate the effect of interpolation on the paleointensity determinations. Firstly, we explore the effect of smoothing the experimental data to assess whether this is a process that reduces noise or not. Then, we test a simplified measuring protocol where half of the heating (alternate Z and I) step values are obtained by interpolation, and we discuss the possibility of interpolating heating steps.

2. Materials and Methods

2.1. Materials

A set of 31 standard paleomagnetic standard cylindrical samples marked, as usual, with an arrow indicating the drill direction, were artificially magnetized with an applied field to simulate the acquisition of an NRM, which from here on will be named TRM_0. The samples were made of different materials, including volcanic rock (VR), slag (S), baked clay (BC), and red (RB), black (BB), and refractory (ReB) bricks. These different materials were obtained from recycled paleomagnetic samples from previously published studies [17–20]. The materials were selected among the recycled samples based on their magnetic stability. The VR samples correspond to dacitic lavas from the Mikri Kameni volcano, the oldest lava flow (1570–1573 eruption) in Nea Kameni, Santorini (Greece). Thermomagnetic measurements [17] indicate two populations of titanomagnetite ($Fe_{3-x}Ti_xO_4$) with high Ti (x = 0.42–52) and a Curie temperature around 250–320 °C and low Ti (x = 0.15) with a higher Curie temperature of 500 °C. The samples plot inside the PSD range on a Day plot [21] and exhibit excellent thermochemical stability. The S samples correspond to slag samples composed of a vitrified mass of silicates from the walls of a limekiln at Calders, north of Barcelona (Spain) [19]. Thermomagnetic curves suggest that the main magnetic carrier is Al- or Ti-substitute magnetite, and susceptibility measurements at different frequencies indicate a predominance of SD grains [19]. The BC samples and some ReB samples were retrieved from the walls of the same limekiln. Magneto-mineralogical characterization indicated similar magnetic carriers but with larger grain sizes, predominantly in the PSD range [19]. The RB samples were obtained from an excavated kiln in a Roman pottery workshop at Alcover, north of Tarragona (Spain) [18], as well as from an isolated Roman kiln that also appeared in a nearby area, at Riera de la Selva (Spain) [20]. The rock magnetic properties of these reddish samples suggested the presence of PSD magnetic grains, as indicated by the corresponding Day plots. There were also signs of low-Ti titanomagnetite in the MD state, evidenced by a relatively sharp Verwey transition at low temperature. This charge-ordering transition appears typically sharp for large and highly crystalline grains. Despite the good thermal reversibility, a tendency for grain agglomeration was observed, as indicated by an increased magnetic susceptibility signal after thermal treatment. Finally, BB samples were obtained from the same pottery workshop at Alcover [18]. The magnetic grains of these blackish samples were also found to be predominantly in the PSD state, and they exhibited a slight tendency toward oxidation, as evidenced by a decrease in magnetic susceptibility after continued thermal treatments.

All the selected paleomagnetic samples displayed good thermal reversibility and were originally used to retrieve successful paleomagnetic intensities. They were recycled as laboratory-magnetized samples that were first heated at high temperature to further thermally stabilize their mineralogy. Then, they were kept at 600 °C for one hour in a Magnetic Measurements MMTD-80 thermal demagnetizer (Magnetic Measurements Ltd., Aughton, UK) with an applied field of 50 μT and, finally, they were allowed to cool down to room temperature under this field. The stability and homogeneity of the applied field were checked with a fluxgate probe. This treatment was intended to erase any previous remanence and to create a new one; additionally, the treatment should have increased the chemical stability of the magnetic grains. The magnetization was not applied in the same direction for all the samples: some samples were placed in the oven with the marked arrow pointing toward the interior of the kiln (in position), some were pointing toward the door (out position), and finally others were not magnetized along the axis of the cylindrical sample; these were placed transversally (trans position) within the sample holder (see Table 1). The aim of imparting magnetization in different directions was to evaluate anisotropy effects.

Table 1. Summary of the features of the 31 standard paleomagnetic samples that were artificially magnetized with an applied field of 50 μT.

Label	Material and Color	Position			Total Samples
		In	Out	Trans	
ReB	refractory brick (yellowish)	5	1	2	8
S	slag (black and porous)	1	3	1	5
BC	baked clay (reddish)	2	1	2	5
VR	volcanic rock (black and porous)	2	1	2	5
RB	brick (reddish)	2	2	2	6
BB	brick (black)	2	0	0	2

From the set of 31 samples, 6 were selected to retrieve the magnetizing field using the standard double-heating Coe variation of the Thellier-type experiment. A field of 50 μT was used for the magnetization (I) steps for three of these samples (ReB1, BC1, BB1); for the other three (ReB2, BC2, BB2), the infield steps were performed using a field of only 30 μT. For these six samples, the measurements after zero field steps show the progressive vanishing of the initial remanence as the temperature increased (Figure 1a), whereas the measurements after the infield steps contain both the remainder of the initial remanence and a newly imparted remanence. The latter can be isolated by vector subtraction of the infield and zero-field remanence values of every temperature step (Figure 1b). The samples were placed in the oven along their axes, and their orientation was reversed between successive applications of the laboratory field (see inset in Figure 1b). This helps to reduce the effects of TRM anisotropy and minimize potential direction biases in remanence acquisition. Finally, all the remanent magnetization values were normalized by dividing them by the initial remanence value to plot the newly acquired TRM versus the remaining original remanence (TRM_0), i.e., reproducing the so-called Arai diagram [7], Figure 1c. By multiplying the slope of a straight line fitted to the points in the Arai plot, one should obtain the field that produced the initial TRM_0.

The remaining 25 samples were left apart to be measured with a simplified measuring protocol consisting of single steps for each temperature, alternatively with zero field (Z) and infield steps (I). From these, 11 were subjected to a field of 50 μT during the infield steps and the remaining 14 to a field of 30 μT. The paleointensity estimation in these cases was performed by direct interpolation of the missing Z points (i.e., interpolation of the remaining TRM_0 or $rTRM_0$) and interpolation of the newly acquired pTRM (which

allows computation of the missing I points). Finally, 2 samples (RB5 and VR3) were remagnetized again (at 600 °C during one hour in a Magnetic Measurements MMTD-80 thermal demagnetizer with an applied field of 50 μT) to repeat a measuring protocol with customized temperature steps.

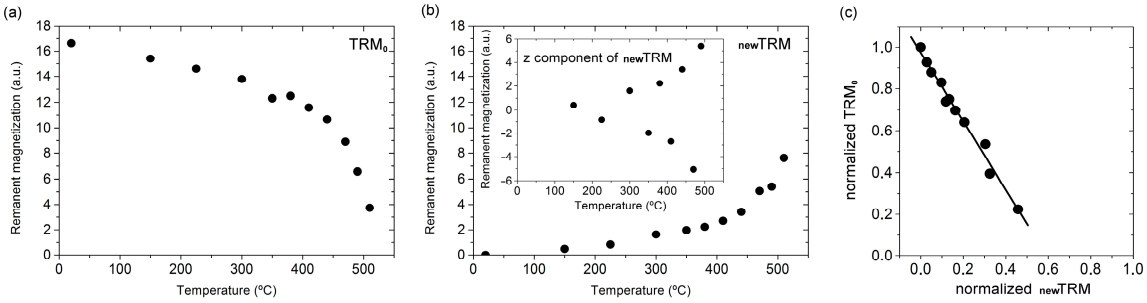

Figure 1. Experimental remanence values obtained for one of the measured samples (ReB2). (**a**) Progressive suppression of the initial remanence by heating under zero field; the original acquired field was imparted during cooling from high temperature under 50 μT. (**b**) Acquisition of a new remanence by heating under an applied field of 30 μT at increasingly high temperatures. (**c**) Arai plot combining both $rTRM_0$ and new pTRM values; the slope multiplied by the applied field (30 μT) produces a good estimate of the initially applied field (50 μT).

All the magnetization measurements were performed on a superconducting rock magnetometer (2G Enterprises, Sunnyvale, CA, USA) available at the Paleomagnetism Laboratory (CCiTUB-CSIC) of the Geosciences Barcelona Institute (Barcelona, Spain). Raw data of the 31 measured samples can be downloaded from the Supplementary Materials Section (Table S1).

2.2. Smoothing and Interpolation Methods

Smoothed data was obtained by modelling the decrease of the initial TRM_0 and the increase of the newly imparted TRM as a function of temperature using different types of functions. Smoothing of the full set of experimental data (measured for the six selected samples) would be justified assuming that the experimental data bears inherent background noise that worsens the precision of the paleomagnetic intensity estimates. Noise is known to be an inherent component of experiments such as those required to produce an Arai plot [22]. Interpolation was also performed using different functions. From them, three were retained, and the corresponding smoothing and interpolation results are presented in this paper.

One of the tested functions was a generalized empirical model of the remanence decay (i.e., the remaining TRM_0 or $rTRM_0$) using a single fitting parameter (n):

$$rTRM_0(T) = (1 - T)^{\frac{1}{n}} \quad (2)$$

The equation can be seen as a simplified form derived from the Arrott–Noakes equation [23]. The variable T is the relative temperature (t/t_{max}), and the n parameter controls the shape of the decay. Assuming that t_{max} is the Curie temperature of the remanence carrier, n could roughly be connected to the degree of concentration of the blocking spectrum near the Curie temperature [24]. The remanence values were normalized to the initial TRM_0 to avoid the need for a term to indicate its value (Figure 2a). On the other hand, the increase of the newly imparted remanence (pTRM) was transformed to allow fitting using the same mathematical expression. For remagnetization data, the pTRM values were transformed to (TRM_0-pTRM)/TRM_0 (where TRM_0 is the initial full remanence magnetization) to get a curve with a shape that resembles a magnetization curve (Figure 2b).

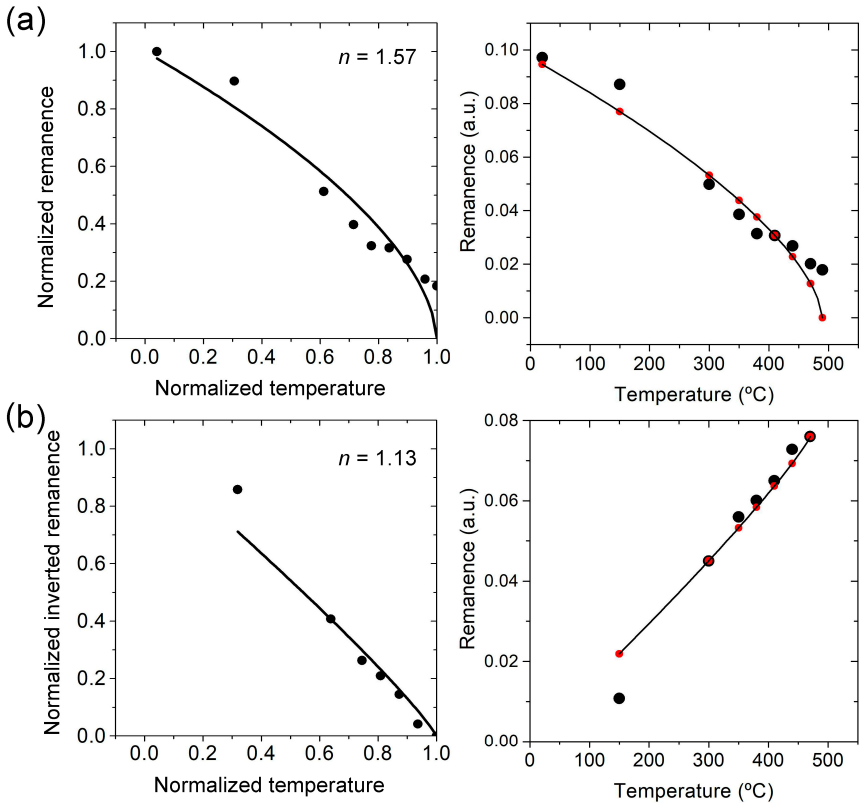

Figure 2. To the left, transformed experimental values of (**a**) demagnetization and (**b**) remagnetization for one of the measured samples (BB1). Transformation enables smoothing the values by fitting them using Equation (2); the fitted n parameter is also shown. To the right, the original data points with smoothed values (in red) and the corresponding fitted function.

Another retained function, with less physical meaning but increased performance, is a modified version of the so-called Five Parameters Logistic (5PL). This function is a variation of the standard dose–response curve, sometimes called the four-parameter logistic equation (e.g., [25]). The modified version of the 5PL function that has been used is

$$RM(t) = P2 + \frac{P1 - P2}{\left(\left(1 + 10^{(t/100 - P3)}\right)^{P4}\right)^{P5}} \quad (3)$$

$RM(t)$ can be both the remaining remanence magnetization ($rTRM_0$) or a newly imparted thermal remanence (pTRM) after $rTRM_0$ subtraction. Logistic functions are not necessarily monotonic; they are usually sigmoidal; therefore, they can contain an inflection point and can adapt better to more complex experimental shapes of $rTRM_0$ and pTRM curves. The 5 parameters can be associated with several features of the sigmoidal curve. $P1$ is the maximum asymptote (maximum remanence), whereas $P2$ is the minimum asymptote (the minimum remanence, which has usually been fixed to 0). $P3$ is the inflection point, and $P4$, also called Hill's slope, relates to the steepness of the curve, and its sign will be negative for demagnetization curves and positive for remagnetization curves. $P5$ is an asymmetry factor [26]; for $P5 = 1$, the curve is a symmetric four-parameter function.

The fitting procedure using either the generalized empirical model or the modified 5PL function was performed using the non-linear least squares fitter tool of Origin 5.0 software [27] based on the Levenberg–Marquardt and Simplex minimization methods.

Finally, an additional method that has been used for interpolation is the spline, namely the cubic Hermite spline [28]. In cubic spline interpolation, every pair of consecutive experimental points is linked with a third-degree polynomial function. In particular, in

cubic Hermite splines, in addition to smoothness in point positions, there is also smoothness in the first derivative, and this enables the overshooting (i.e., unwanted oscillations) control, preserving monotonicity between every pair of points. The interpolator is a linear combination of four basic functions:

$$H(t) = h_1(t)\cdot f_1 + h_2\cdot f_2(t) + h_3(t)\cdot f'_1 + h_4\cdot f'_2 \quad (4)$$

f_1 and f_2 are the remanence values of the endpoints within the interpolated segment.
f'_1 and f'_2 are the first derivatives of the two endpoints.
h_1, h_2, h_3, h_4 are the Hermite basic functions, defined as

$$h_1 = 1 - 3p^2 + 2p^3$$

$$h_2 = 3p^2 - 2p^2$$

$$h_3 = p - 2p^2 + 3p^3$$

$$h_4 = p^2 + p^3$$

p values are within the interval [0, 1], defined as

$$p = \frac{t - t_1}{t_2 - t_1}$$

Cubic Hermite interpolation was computed using a Python 3.11 code (using the PchipInterpolator class within the SciPy.interpolate package) under the Jupyter Notebook 6.5.4 interactive computing platform. The required first derivatives were approximated using central differences.

3. Results and Discussion

3.1. Standard Double-Heating Coe Method

The six samples measured using the standard double-heating Coe variation of the Thellier experiment produce intensity values (Table 2) close to the known applied field (50 μT). This confirms the competence of the method to produce good paleointensity estimates when applied to samples bearing an isotropic dilution of stable magnetic particles. It is usually accepted that the best estimates are obtained with a newly imparted TRM with a field close to the one that produced the original NRM [24,29]. However, the results highlight that the number of heating steps is also a very important factor. Indeed, the Arai plots for samples measured with 30 μT infield steps were built with eleven/ten temperature steps instead of the eight used for samples measured with 50 μT infield steps. This results in higher quality factors for the experiments performed with 30 μT infield steps.

3.2. Smoothed Data in Standard Double-Heating Coe Method

The smoothed values computed using Equations (2) and (3) should suppress part of the experimental noise registered in the demagnetization ($rTRM_0$) and remagnetization (pTRM) experiments. This noise would be due to random and uncontrolled factors, and its suppression should result in Arai plots with better quality factors and improved field estimates. However, smoothing is not a common practice in paleointensity determinations, and it has been applied only rarely. For instance, in [30], a three-point sliding average was applied to NRM and TRM values. Despite being based on an empirical model of the remanence decay, the smoothed values using Equation (2) result in Arai plots that lead to magnetic field estimates that differ significantly from the magnetizing field (50 μT) (see red

values within Figure 3 and Table 3). This divergence implies that not all the irregularities observed in the experimental de- and remagnetization curves are really noise.

Table 2. Original magnetizing field estimates obtained by applying the standard measuring protocol. Columns from left to right: Sample, label of the specimen identifying the nature of the sample; F_{lab}, applied field during infield heating steps; T range, temperature range from the first to the last heating steps; F, intensity estimate; ΔF%, deviation percentage from the original imparted field (50 μT); σ, standard deviation of the intensity estimate; n, number of heating steps used for the intensity determination; f, fraction of original magnetization used for intensity determination; g, gap factor; and q, quality factor as defined by [15].

Sample	F_{lab} (μT)	T Range (°)	F (μT)	ΔF%	σ (μT)	n	f	g	q
BC1	50	20–470	52	4	7.8	8	0.82	0.73	6.68
BC2	30	20–510	48	−4	1.0	11	0.99	0.83	49.90
ReB1	50	20–470	52	4	8.3	8	0.67	0.78	6.33
ReB2	30	20–510	50	0	3.1	11	0.77	0.86	16.02
BB1	50	20–470	51	2	3.1	8	0.79	0.71	16.52
BB2	30	20–510	48	−4	2.5	10	0.86	0.74	19.13

Table 3. Comparison of the magnetizing field estimates obtained by applying the standard measuring protocol and using interpolated values using Equations (2) and (3). For every estimate, in addition to the magnetizing field (F), deviation percentages (ΔF%) from the original imparted field (50 μT), standard deviations (σ), and quality factors (q), as defined by [15] are also shown. The last row indicates the average values and their associated uncertainties.

Sample	Not Smoothed				Smoothed Using (2)				Smoothed Using (3)			
	F (μT)	ΔF%	σ (μT)	q	F (μT)	ΔF%	σ (μT)	q	F (μT)	ΔF%	σ (μT)	q
BC1	52	4	7.8	6.68	42	−16	11.4	3.67	51	2	6.5	7.83
BC2	48	−4	1.0	49.90	46	−8	0.4	130.30	48	−4	1.1	41.85
ReB1	52	4	8.3	6.33	57	14	3.6	16.10	53	6	4.7	11.34
ReB2	50	0	3.1	16.02	64	28	3.7	17.41	47	−6	1.8	26.88
BB1	51	2	3.1	16.52	60	20	5.9	10.13	51	2	1.9	27.81
BB2	48	−4	2.5	19.13	57	14	2.5	22.78	45	−10	3.8	11.66
mean	50.2		4.3		54.3		4.6		49.2		3.3	

As Equation (2) is monotonic, and it has only a single adjustable parameter, it cannot adapt to the irregularities of the experimental $rTRM_0$ and pTRM curves. These irregularities indicate that the remanence carriers of the samples are a complex mixture of grain sizes, perhaps including different magnetic minerals. In contrast, the 5PL function is more versatile; it can be sigmoidal and adapts better to the experimental values (see blue values within Figure 3). Compared to the values obtained using Equation (2), those using Equation (3) produce field estimates much closer to the magnetizing field (see Table 3). However, these estimates are not better than those obtained using the non-smoothed values (except for sample BC1); they are actually slightly worse. Sample BB2 deserves a special comment: this sample exhibits a sharp blocking/unblocking behavior, and even Equation (3) fails to reproduce the known magnetizing field (ΔF% = −10%). Therefore, the advantage of the smoothed values using the 5PL equation is not better field estimates, but smaller standard deviations and, consequently, higher quality factors. This was an expected result for smoothed data, though not achieved using Equation (2). In contrast, comparing the results

for non-smoothed and smoothed values using Equation (3) (see Table 3), the standard deviation and quality factor improve for four out of the six studied samples. Average values point to the same conclusions.

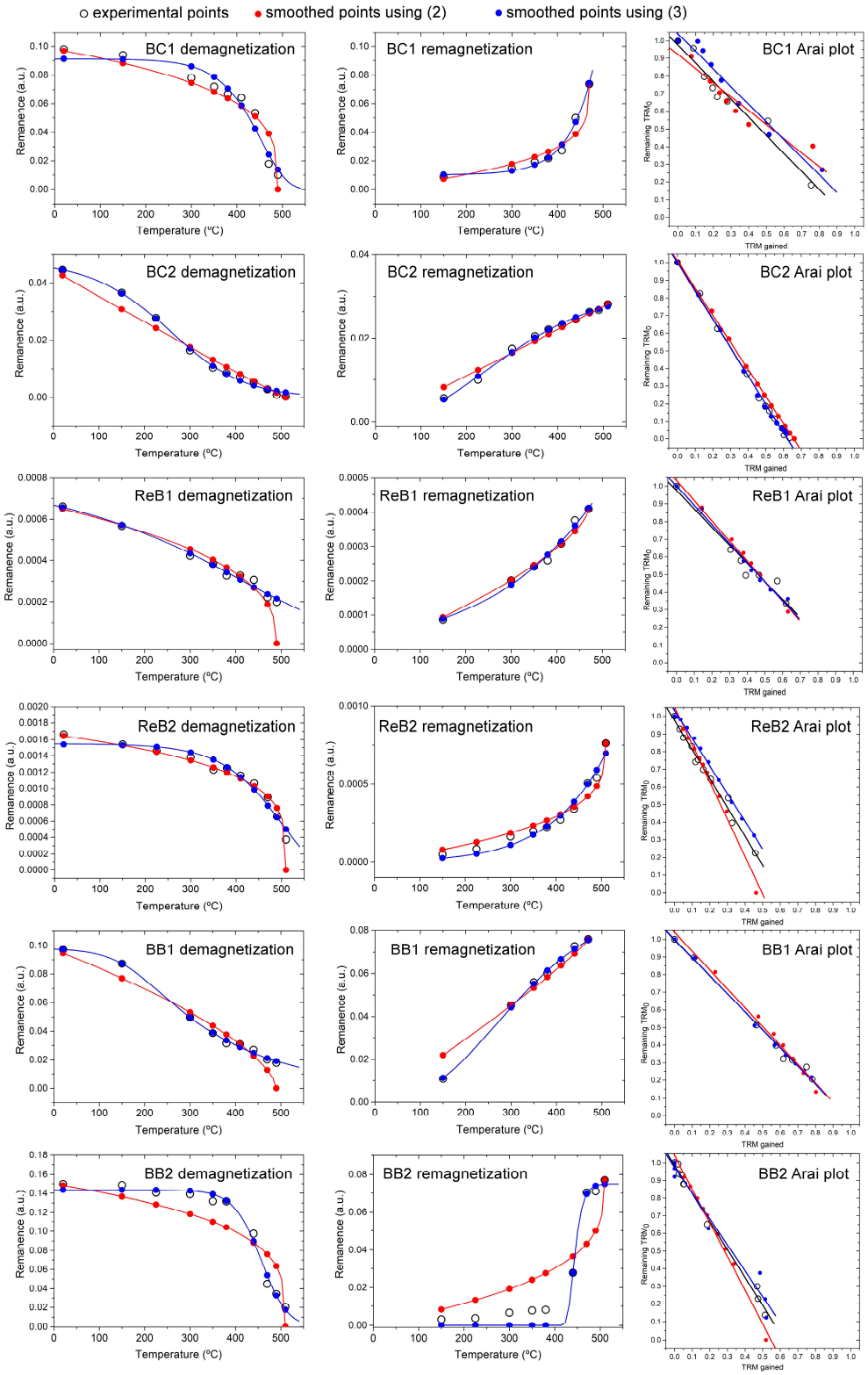

Figure 3. Experimental (open dots) and smoothed values using Equation (2) in red and Equation (3) in blue for the six samples measured following the standard double-heating Coe measuring protocol. To the (**left**), the demagnetization curves; in the (**middle**), the remagnetization curves; and to the (**right**), the resulting Arai plots, where the points have been fitted to a straight line using the same color code.

3.3. Interpolated Data in Single-Step Heating Method

In the previous section, it was concluded that the smoothed values (using the 5PL function) produce similar field estimates to the experimental (non-smoothed) values, and, in general, smaller standard deviations and higher quality factors. Indeed, the fitted 5PL functions not only allow for computing smoothed values but also any other additional value within the studied range (i.e., interpolated data). Using interpolated data, the quality factors can be increased indefinitely; see, e.g., Table 4. Clearly, the massive use of interpolated points has negative effects; for instance, the field estimate could appear more precise than it is, and accuracy is not really increased. Such interpolation could be criticized as a fabricated and unjustified enhancement of the experimental data.

Table 4. Comparison of the magnetizing field estimates (F) and, particularly, the standard deviations (σ) and quality factors (q) as defined by [15] for the experimental and the 5PL computed values (smoothed and interpolated) corresponding to sample BB1. N is the number of points considered, and this could be extended indefinitely by adding more and more interpolated points.

	N	F (μT)	σ (μT)	q
experimental	8	51	3.1	16.5
smoothed	8	51	1.9	27.8
interpolated	16	52	0.9	58.3
interpolated	46	52	0.5	110.0
interpolated	91	52	0.3	158.9

In the case of sample BB1 (Table 4), the smoothed values using Equation (3), i.e., the 5PL, produce a field estimate (51 μT) comparable to that obtained using experimental values and very close to the true magnetizing field (50 μT), but in general (see Table 3), the field estimates using 5PL smoothed values are slightly further from the true magnetizing field. Taking into account that the 5PL smoothed values do not add accuracy to the field estimates, an alternative to smoothing is the use of a spline (see Equation (4) in Section 2.2), i.e., a mathematical function used only to interpolate values within the studied magnetization range but leaving untouched the experimental values.

To check the convenience of using interpolation with or without smoothing, the data from the three samples that were remagnetized under a 30 μT field (BC2, ReB2, BB2) were used to simulate a simplified measuring protocol consisting of single steps for each temperature, alternatively with zero field (Z) and infield (I) steps (i.e., for every temperature only a Z or I measurement was considered and the corresponding (I or Z) steps were interpolated either using the 5PL function (Equation (3)) or cubic Hermite splines (Equation (4)). The experimental (Z or I) steps were smoothed (when using 5PL approach) or simply taken as they are (when using cubic Hermite splines). The results (Table 5) seem to indicate that the use of cubic Hermite splines produces more accurate results (closer to the true original magnetizing field of 50 μT), although with lower quality factors (lower precision) because the resulting Arai plots exhibit loose linearity (Figure 4). Sample BB2 deserves a special mention; the use of fewer experimental points affects particularly the shape of the remagnetization curve at a higher temperature (compare the remagnetization curves of the BB2 sample in Figures 3 and 4), and the oversimplified exponential remagnetization curve results in a clearly concave-up Arai plot that produces an underestimated magnetizing field (see Table 5). Please note that this concavity is due to interpolation and is not an indicator of the MD behavior. For this particular sample, there is almost no difference between using the 5PL function and the cubic Hermite splines.

Table 5. Comparison of the magnetizing field estimates (F) obtained by applying the single-step heating method that requires interpolation of the missing steps using either the 5PL function (left) or cubic Hermite splines (right). The experimental points were additionally smoothed when using the 5PL function. N is the number of considered temperature steps (combining a ZI pair formed by an experimental (or smoothed) measurement and an interpolated one). Deviation percentages (ΔF%) from the original imparted field (50 μT), standard deviations (σ), and quality factors (q), as defined by [15], are also shown.

Sample	5PL Smoothing and 5PL Interpolation					Cubic Hermite Spline Interpolation			
	N	F (μT)	ΔF%	σ (μT)	q	F (μT)	ΔF%	σ (μT)	q
BC2	11	50	0	0.7	71.9	49	−2	1.2	41.2
ReB2	11	59	18	3.2	18.5	54	8	3.5	15.3
BB2	11	46	−8	6.0	7.6	46	−8	6.0	7.6

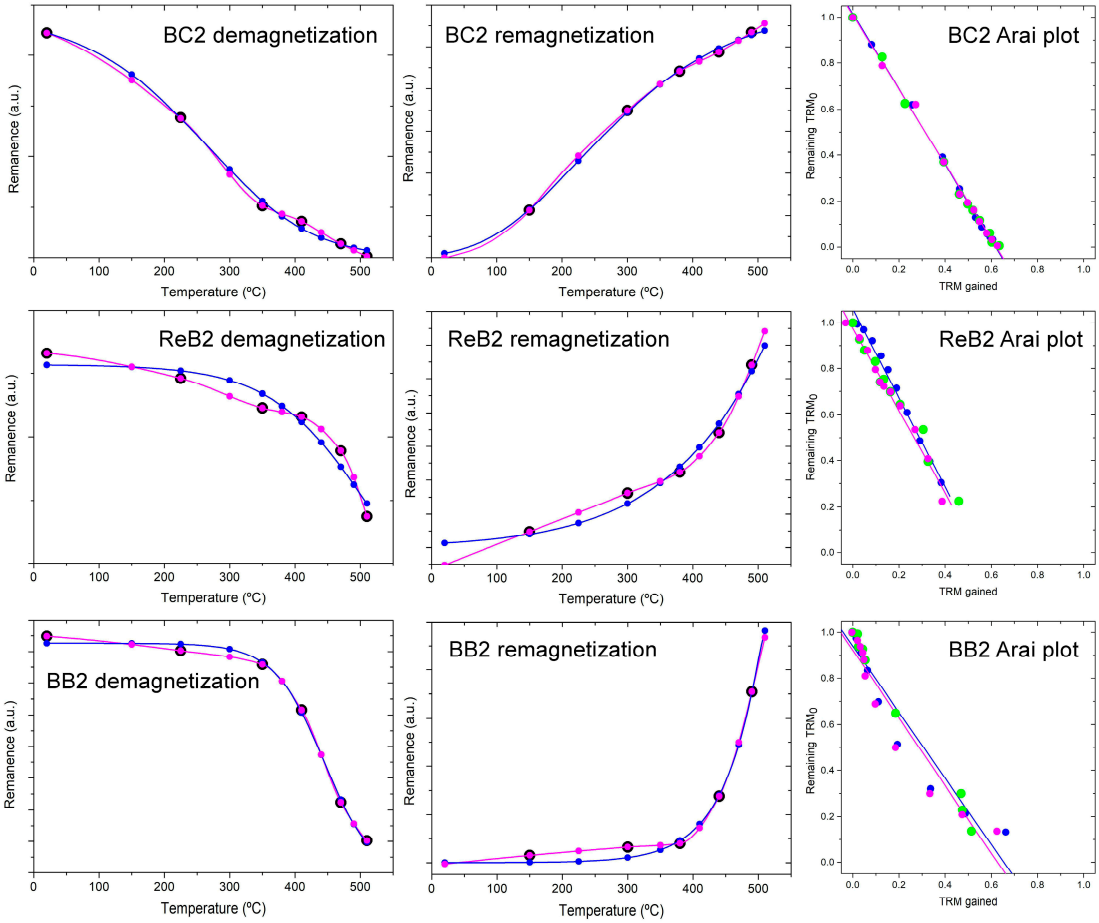

Figure 4. Simulated one-step experiments for samples BC2, ReB2, and BB2. Only interspersed experimental demagnetization and remagnetization data (black dots) were taken into account, and the corresponding temperature steps were interpolated using either the 5PL function (blue) or cubic Hermite splines (magenta). Experimental points were additionally smoothed when using the 5PL function (please note that the blue points do not match exactly with the black dots). To the (**left**), the demagnetization curves; in the (**middle**), the remagnetization curves; and to the (**right**), the resulting Arai plots, where the points have been fitted with a straight line using the same color code. For comparison, the experimental Arai plot (obtained following the double-heating protocol) is also shown using green dots.

The single-step heating method was finally tested systematically for 25 paleomagnetic samples using cubic Hermite splines to interpolate the "missing" Z and I steps. Please note that I steps were not directly interpolated. In fact, for these infield steps, the interpolated values correspond to the gained pTRM. Therefore, the corresponding (and interpolated) Z steps were first subtracted from the measured infield step. It is worth mentioning that here, interpolating I steps involves already interpolated values (from Z steps). The direction of the interpolated Z steps has been assumed to match the mean direction obtained using all the experimentally measured Z steps.

All the measured samples but three produced Arai plots with more-or-less aligned points (see some examples in Figure 5; all Arai plots can be found in Table S1). The plots from four samples (ReB3, ReB4, VR4, and VR5) are not strictly linear, and their resulting field estimates can be questioned. For the rest of the samples, their estimates can be considered reasonable, accurate, and precise, and relatable to the original magnetizing field (50 μT) regardless of the applied field (30 or 50 μT) (see Table 6 and Figure 6). The position of the samples (in, out, trans) does not appear to affect the quality of the intensity estimates. Samples with a newly imparted TRM colinear with the original TRM_0 do not exhibit systematically smaller ΔF% values. This suggests that the direction of the TRM does not significantly influence the quality of the estimates, indicating that TRM anisotropy is not significant in the analyzed samples. The field estimate (F) is usually just above 50 μT. However, for 5 samples the value is below 50, particularly low for 2 of these samples (BC5 and ReB8). For 17 out of the 25 tested samples, the F values differ from the original imparted field (50 μT) by less than 12%, which is close to the typical margins of error in intensity estimates dealing with potsherds and baked brick samples [31,32]. In some cases, the s.d. is very low and the corresponding quality factor (q) is very high. In particular, sample BC4 has a q value of 32. Despite the lack of consensus on the quality threshold for paleointensity data [33], values of $q > 10$ are usually considered to be high-quality estimates (eight samples produced estimates with $q > 10$). Also, $q > 5$ is often considered an indicator of acceptable and reliable estimates. However, the threshold to select data can be placed even at lower values, such as $q > 1$ [34,35]. Here, all the measured samples can be considered high quality, as only four samples produced q values below 5. In any case, even the Arai plots with $q < 5$ produce estimates that are very close or relatively close to the original magnetizing field. However, it is worth noting that q (along with other quality indicators) is subject to the effects of interpolation, which also affects their common interpretation. The slag (S) and volcanic (VR) samples are the ones that appear to produce estimates that are systematically biased toward values slightly above 50 μT; this correlates with a higher Fe content for these samples. Perhaps a minor chemical alteration could explain the systematic (though subtle) overestimation of the magnetizing field. The two samples with a clear underestimation of the magnetizing field (BC5 and, especially, ReB8) have high quality factors, and therefore, it would be misleading to use these two results to assess the field. It is difficult to know whether the underestimation could be attributed solely to the nature of the one-step heating method or not. In conventional Thellier-type paleointensity determinations, thermal alteration and multidomain grains are known causes of underestimation. In fact, for one of the samples (ReB8), the Arai plot exhibits an abrupt change of the slope (see ReB8 in Figure 5) that could indicate thermal alteration. This sample was hard to demagnetize at the beginning, and then, from 440 °C onwards, it demagnetized much more quickly, and the slope within the Arai plot decreases. The slope omitting the last three points (≥440 °C) yields a magnetizing field estimate of 50.9 μT.

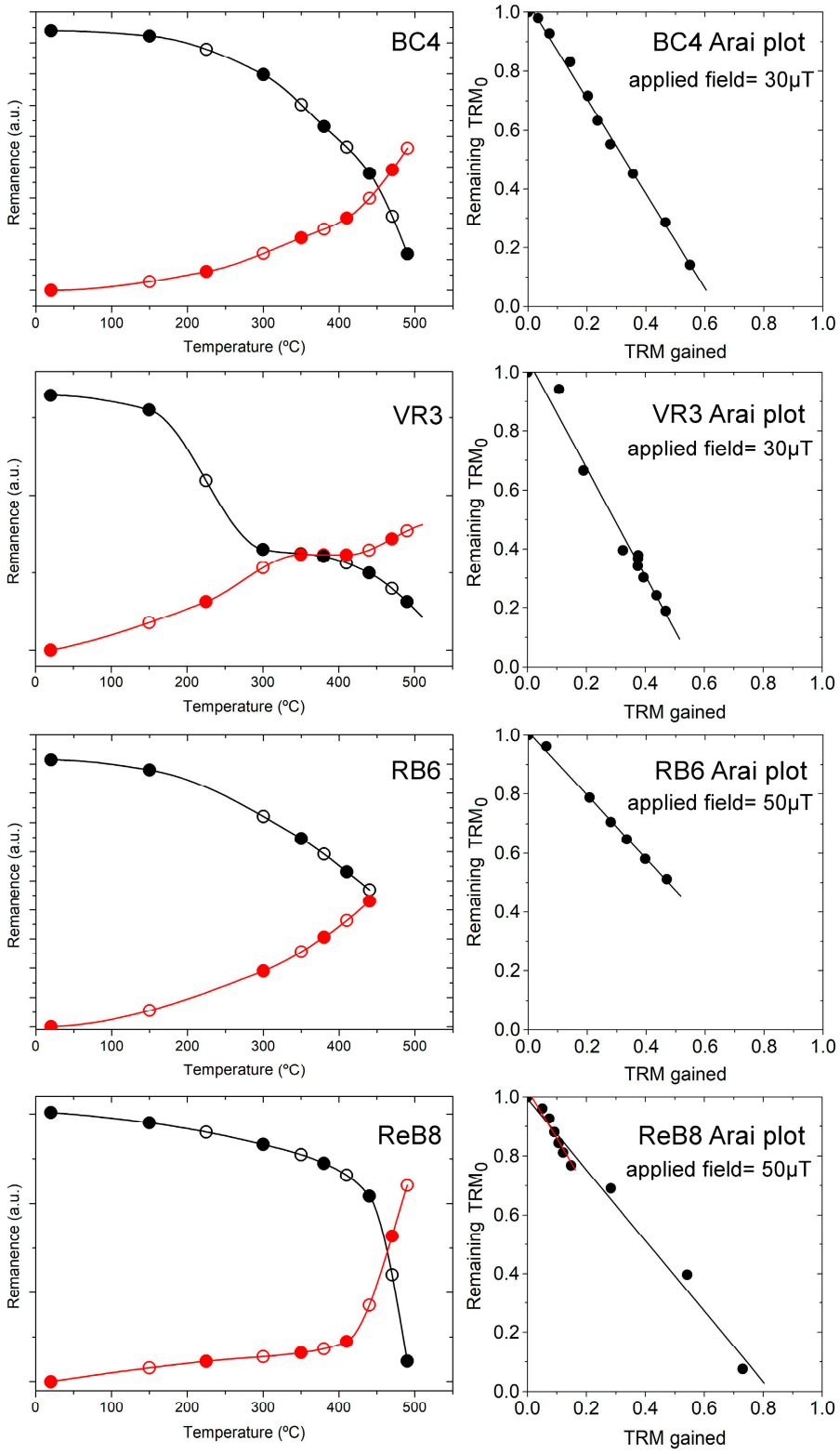

Figure 5. Single-step heating experiments for samples BC4, VR3, RB6, and ReB8. On the (**left**), demagnetization (black) and remagnetization (red) curves. The experimental points are depicted as solid dots and the interpolated points as open dots. On the (**right**), the corresponding Arai plots and the corresponding linear fit; for sample ReB8, a linear fit excluding the last three points is also shown in red.

Table 6. Magnetizing field estimates (F) obtained by applying the single-step heating method, interpolating the missing steps using cubic Hermite splines. Deviation percentages (ΔF%) from the original imparted field (50 μT), standard deviations (σ), and quality factors (q) and (f), as defined by [15], are shown. The position of the samples within the oven during the starting magnetization that produced the TRM_0 is also indicated. Labels including an asterisk indicate non-linear Arai plots.

Label	Position	N	Applied Field (μT)	F (μT)	ΔF%	σ (μT)	q	f
BC3	trans	7	50	55.7	11.4	7.2	7.8	0.7
BC4	trans	10	30	48.6	−2.8	1.5	32.0	0.9
BC5	in	10	30	42.4	−15.2	3.3	12.9	0.8
RB1	trans	9	30	52.6	5.2	8.0	6.6	0.4
RB2	out	-	30	-	-	-	-	-
RB3	in	10	30	49.6	−0.8	4.9	10.1	0.7
RB4	trans	7	50	53.4	6.8	6.9	7.8	0.3
RB5	out	7	50	51.0	2.0	3.7	13.9	0.3
RB6	in	7	50	53.7	7.4	3.0	17.8	0.5
ReB3*	in	7	50	54.3	8.6	11.2	4.8	0.7
ReB4*	trans	10	30	55.1	10.2	6.4	8.6	0.5
ReB5	trans	7	50	46.5	−7.0	5.6	8.3	0.6
ReB6	out	10	30	50.4	0.8	11.9	4.2	0.8
ReB7	in	10	30	51.8	3.6	5.1	10.1	0.7
ReB8	in	10	30	36.4	−27.2	2.3	16.13	0.9
S1	out	7	50	53.5	7.0	7.1	7.5	0.8
S2	in	7	50	55.6	11.2	10.2	5.5	0.6
S3	out	10	30	58.1	16.2	5.7	10.2	0.7
S4	trans	7	50	58.4	16.8	7.2	8.1	0.9
S5	out	10	30	55.9	11.8	6.2	9.0	0.7
VR1	trans	-	50	-	-	-	-	-
VR2	in	-	50	-	-	-	-	-
VR3	trans	10	30	56.0	12.0	4.8	11.7	0.8
VR4*	out	10	30	60.0	20.0	12.5	4.8	0.9
VR5*	in	10	30	55.6	11.2	6.1	9.1	1.0

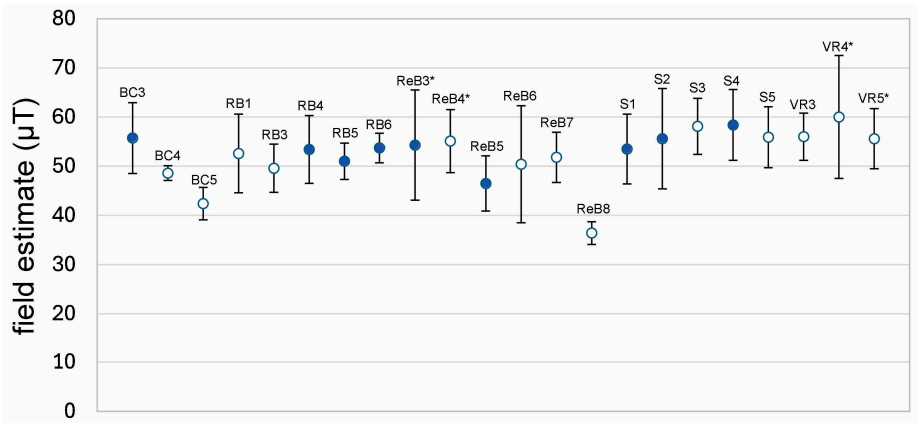

Figure 6. Error bar plot showing the magnetizing field estimates (F) listed in Table 6, including samples remagnetized with a 50 μT field (solid dots) and a 30 μT field (open dots). Labels including an asterisk indicate non-linear Arai plots.

In addition to BC5 and ReB8, three other samples showed significant deviations (overestimation > 15%) from the imparted field (VR4, S3, and S4). Notably, S3 and S4 have relatively good q values. The causes of these inconsistencies remain unclear. They may be inherent to specific characteristics of these samples, despite their careful selection, or they may suggest that, for these samples, the interpolated data do not adequately replace the experimental data that would have been obtained using the standard double-heating method.

When comparing by type of sample, baked clay (BC) and refractory brick (ReB) exhibit the highest degree of scatter. This is partly due to the previously mentioned BC5 and ReB8 samples and may suggest that these two types of materials do not magnetize as uniformly as the others tested.

Only 3 out of the 25 measured samples failed to produce estimates of the magnetizing field (i.e., non-linear, not even convex but simply noisy Arai plots). These are, on the one hand, two volcanic samples (VR1 and VR2) that demagnetized too quickly (after the second Z heating step, 70% of the original TRM_0 was gone) and exhibited hints of acquiring viscous remanence. On the other hand, for one red brick sample (RB2), the problem was the opposite. This sample showed an anomalously high resistance to demagnetization (at 490 °C only 46% of the TRM_0 had been erased); therefore, the computed Arai plot has a very low f factor (0.39), and the first heating steps only add noise to the computation of the slope.

As a whole, the failure rate for the investigated samples (omitting convex Arai plots) would be 12%, which is fairly low [36]. This low rate is logical, taking into account that the selected samples to be artificially magnetized were previously thermally stabilized. Thermal alteration should be minimal for them, but a certain failure rate could still be expected due to non-ideal magnetic properties. As previously stated, hints of a certain degree of alteration have also been found for sample ReB8, and for four other samples, the Arai plots are not strictly linear. Yet, the success rate is as high as expected for previously treated samples.

The single-step heating method presented here is not intended to substitute existing methods; rather, it is intended to illustrate the possibility of obtaining acceptable (even high-quality) Arai plots and field estimates by interpolating a large number of Z and I steps. The tested samples were of different types, and they were heated together in a single sample boat. By personalizing the heating steps for every type of sample, the results could be substantially improved. Please note that volcanic samples tend to demagnetize easily, and, in contrast, red and refractory brick samples tend to be harder to demagnetize. For some samples, the quality factor could have been increased by extending the measurements to higher temperatures, covering a larger portion of the TRM_0 (i.e., increasing the f factor). One volcanic rock sample (VR3bis) and a brick sample (RB5bis) were remagnetized again under a field of 50 μT and remeasured using customized heating steps. This resulted in better Arai plots with a more homogeneous distribution of points that covered essentially the full range of demagnetization. The results are presented in Figure 7, and they include pTRM and tail checks. These can be intercalated in the single-step protocol as follows: after an infield (I) experimental step, an additional I step is performed, heating at a lower temperature, followed by a zero-field (Z) step at the previous highest temperature. These provide the values needed to calculate the pTRM and the pTRM tail checks, respectively. The additional I step can be compared to either an experimental step or to an interpolated value if no direct measurement is available. As for the additional Z step, this should be subtracted from the corresponding interpolated Z step to determine the tail. Alternatively, pTRM tail checks can be performed following an experimental Z step, thereby avoiding the use of interpolated values. Anisotropy and cooling rate corrections were not applied

because the cooling rate during the measuring protocol was the same during the starting magnetization (to impart TRM_0) and the magnetization direction was always along the axis of the cylindrical samples. However, both corrections should be applied, as is standard in conventional double-step measurements for real (not laboratory-magnetized) samples.

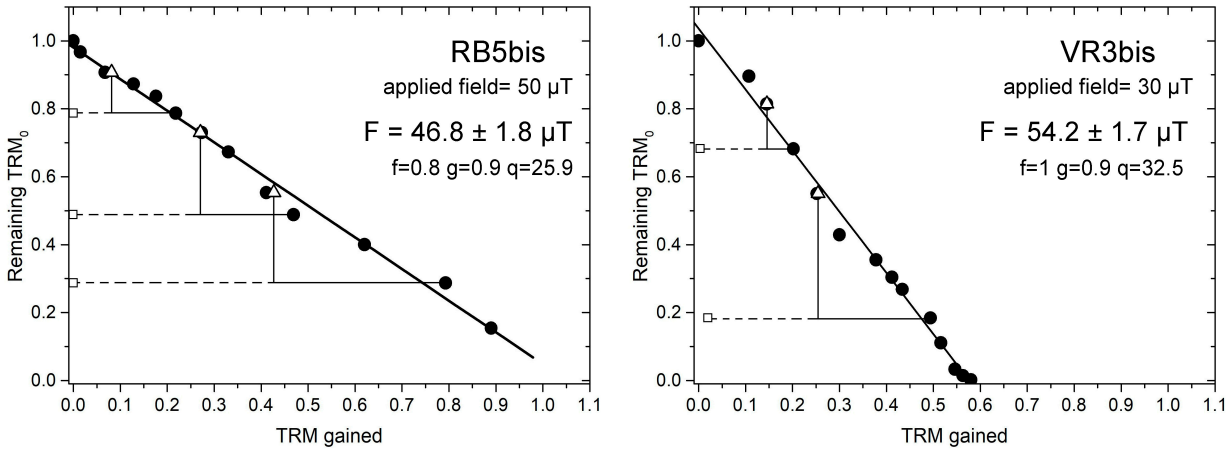

Figure 7. Arai plots corresponding to single-step heating experiments for samples RB5bis and VR3bis. The heating steps were customized for these two samples (see experimental details in Table S1), resulting in improved quality factors; pTRM and pTRM tail checks were also measured.

The two remeasured samples display highly linear Arai plots along the full measured range. This range covers almost the full portion of the TRM_0 (f is actually 1 for VR3bis) with a high degree of evenness of the heating steps. This results in very high q values and a very small standard deviation (<2 μT). Table 7 shows the results for these two samples with (bis samples) and without customized heating steps. Despite the improved quality factors, the field estimate (F) is not substantially closer to the original magnetizing field (50 μT), and for sample RB5, the estimate is even further from the true field. This indicates that an increased precision in the method does not imply an increased accuracy. The results suggest that the single-heating method, as expected, would have a worse accuracy than the standard double-heating method, and the overall results would possibly show a higher scattering. Nevertheless, the method could be used to enlarge a dataset of estimates combining sister specimens measured using the conventional double-heating protocol and others with the faster single-heating method.

Table 7. Comparison of the results for RB5 and VR3 and the remeasured RB5bis and VR3bis samples. Magnetizing field estimates (F) were obtained by applying the single-step heating method, interpolating the missing steps using cubic Hermite splines; N temperature steps were considered. Deviation percentages (ΔF%) from the original imparted field (50 μT), standard deviations (σ), and quality factors (f), (g), and (q), as defined by [15], are shown.

Label	N	Applied Field (μT)	F (μT)	ΔF%	σ (μT)	f	g	q
RB5	7	50	51.0	2.0	3.7	0.3	0.8	13.9
RB5bis	13	50	46.8	6.4	1.8	0.8	0.9	25.9
VR3	10	30	56.0	12.0	4.8	0.8	0.8	11.7
VR3bis	14	30	54.2	8.4	1.7	1.0	0.9	32.5

4. Conclusions

Several procedures have been tested to smooth and interpolate measuring steps in both demagnetization (Z steps) and remagnetization (leading to I steps) curves in Thellier-type paleointensity determinations.

With regard to smoothing procedures, they have been found to improve the paleomagnetic field estimate and the associated quality factors of the corresponding Arai plot only rarely. A function with only a single adjustable parameter (a generalized empirical model of the remanence (Equation (2)) fails to effectively model the demagnetization/remagnetization curves. This would imply that most of the irregularities observed in the experimental curves are not noise, but a genuine feature produced by complex assemblies of remanence carriers. A function with more adjustable parameters (a modified version of the 5PL function (Equation (3)) adapts better to the irregularities of the magnetization curves suggested by the experimentally measured values. Smoothing using the 5PL function results in field estimates of good quality, but not of better quality than those obtained experimentally (i.e., without any smoothing). Therefore, despite the different experimental sources of noise [22], smoothing appears to be a worthless procedure in Thellier-type paleointensity determinations, and the procedure could actually obscure physically meaningful data.

With regard to interpolation procedures, cubic Hermite splines (Equation (4)) have been demonstrated to be an effective way to compute interpolated Z or I steps. By interpolation, the number of points in the Arai plot can be increased artificially and indefinitely. Such an increase would affect positively some of the Coe's quality parameters, in particular decreasing the scatter (β) and increasing the quality (q) factors. However, this would be a fabricated enhancement that most paleomagnetists would criticize as unjustified. Some justification for interpolation can be found in the presented single-step heating method to obtain ancient field estimates. The presented alternative method is a hybrid approach that combines experimental and interpolated steps, and it has proven efficient to obtain relatively reliable field estimates. However, interpolation has some undesired effects; Arai plots can appear more scattered, resulting in more scattered overall results. The single-step heating method would not be applicable for retrieving reliable ancient field intensities on its own. The method could be used to save measuring time, increasing the number of studied specimens when sister specimens measured using the conventional double-heating protocols have already exhibited usefulness for intensity determinations. Furthermore, this alternative method would be a way to explore in a more continuous way the blocking temperature spectra of the measured samples without increasing the experimental measuring time. Therefore, the method might be of use for samples bearing complex assemblies of remanence carriers because it allows the retrieval of information from a higher number of temperatures for a given number of heating steps. However, the implementation of the single-step method to paleointensity studies should also include the conventional MD and alteration checks, as well as anisotropy and cooling rate corrections.

In addition to the use of interpolation as a part of the presented single-step method, interpolation could also be used occasionally to detect/address noisy points affected by experimental errors, or other uncontrolled issues, within the Arai plot, or to compute a heating step that was involuntarily skipped.

Supplementary Materials: The following supporting information can be downloaded at https://www.mdpi.com/article/10.3390/min15080873/s1: Table S1: raw data corresponding to the remanent magnetization measurements from the 31 magnetized samples.

Author Contributions: Conceptualization, L.C.; experimental work, L.C. and M.O.; formal analysis, L.C. and R.D.F.; interpretation, L.C.; writing—original draft preparation, L.C.; writing—review and editing, all authors. All authors have read and agreed to the published version of the manuscript.

Funding: Financial support from project CGL2013-42167-P (Spanish Ministerio de Economía y Competitividad) is acknowledged.

Data Availability Statement: Most of the data presented in this study have been made publicly available. Any other data are available on request from the corresponding author.

Acknowledgments: We would like to thank the editor as well as the anonymous reviewers for their valuable remarks and comments.

Conflicts of Interest: Author Marc Ortiz was employed by the company Geo-Min. The remaining authors declare that the research was conducted in the absence of any commercial or financial relationships that could be construed as a potential conflict of interest.

References

1. Thellier, E.; Thellier, O. Sur l'intensité Du Champ Magnétique Terrestre Dans Le Passé Historique et Géologique. *Ann. Géophys.* **1959**, *15*, 285–376.
2. Thellier, E. Sur La Thermoremanence et La Theorie Du Metamagnetisme. *C. R. Acad. Sci. Paris* **1946**, *223*, 319–321.
3. Shaar, R.; Tauxe, L. Thellier GUI: An Integrated Tool for Analyzing Paleointensity Data from Thellier-Type Experiments. *Geochem. Geophys. Geosyst.* **2013**, *14*, 677–692. [CrossRef]
4. Selkin, P.A.; Gee, J.S.; Tauxe, L. Nonlinear Thermoremanence Acquisition and Implications for Paleointensity Data. *Earth Planet. Sci. Lett.* **2007**, *256*, 81–89. [CrossRef]
5. Coe, R.S. Paleo-Intensities of the Earth's Magnetic Field Determined from Tertiary and Quaternary Rockstle. *J. Geophys. Res.* **1967**, *72*, 3247–3262. [CrossRef]
6. Zijderveld, J.D.A. AC Demagnetization of Rocks: Analysis of Results. In *Methods in Paleomagnetism*; Collinson, D.W., Creer, K.M., Eds.; Elsevier: Amsterdam, The Netherlands, 1967; pp. 254–286.
7. Nagata, T.; Momose, K.; Arai, Y. Secular Variation of Geomagnetic Total Force during Last 5000 Years. *J. Geophys. Res.* **1963**, *68*, 5277. [CrossRef]
8. Aitken, M.J.; Alcock, P.A.; Bussell, G.D.; Shaw, C.J. Archaeomagnetic Determination of the Past Geomagnetic Intensity Using Ancient Ceramics: Allowance for Anisotropy. *Archaeometry* **1981**, *23*, 53–64. [CrossRef]
9. Hervé, G.; Chauvin, A.; Lanos, P.; Rochette, P.; Perrin, M.; Perron d'Arc, M. Cooling Rate Effect on Thermoremanent Magnetization in Archaeological Baked Clays: An Experimental Study on Modern Bricks. *Geophys. J. Int.* **2019**, *217*, 1413–1424. [CrossRef]
10. Muxworthy, A.R.; Baker, E.B. ThellierCoolPy: A Cooling-Rate Correction Tool for Paleointensity Data. *Geochem. Geophys. Geosyst.* **2021**, *22*, e2021GC010145. [CrossRef]
11. Dunlop, D.J.; Özdemir, Ö. *Rock Magnetism: Fundamentals and Frontiers*; Cambridge University Press: Cambridge, UK, 1997; ISBN 9780521000987.
12. Levi, S. The Effect of Magnetite Particle Size on Paleointensity Determinations of the Geomagnetic Field. *Phys. Earth Planet. Inter.* **1977**, *13*, 245–259. [CrossRef]
13. Tauxe, L.; Santos, C.N.; Cych, B.; Zhao, X.; Roberts, A.P.; Nagy, L.; Williams, W. Understanding Nonideal Paleointensity Recording in Igneous Rocks: Insights from Aging Experiments on Lava Samples and the Causes and Consequences of "Fragile" Curvature in Arai Plots. *Geochem. Geophys. Geosyst.* **2021**, *22*, e2020GC009423. [CrossRef]
14. Brown, M.C.; Hervé, G.; Korte, M.; Genevey, A. Global Archaeomagnetic Data: The State of the Art and Future Challenges. *Phys. Earth Planet. Inter.* **2021**, *318*, 106766. [CrossRef]
15. Coe, R.S.; Grommé, S.; Mankinen, E.A. Geomagnetic Paleointensities from Radiocarbon-Dated Lava Flows on Hawaii and the Question of the Pacific Nondipole Low. *J. Geophys. Res. Solid Earth* **1978**, *83*, 1740–1756. [CrossRef]
16. Riisager, P.; Riisager, J. Detecting Multidomain Magnetic Grains in Thellier Palaeointensity Experiments. *Phys. Earth Planet. Inter.* **2001**, *125*, 111–117. [CrossRef]
17. Spassov, S.; Valet, J.-P.; Kondopoulou, D.; Zananiri, I.; Casas, L.; Goff, M.L. Rock Magnetic Property and Paleointensity Determination on Historical Santorini Lava Flows. *Geochem. Geophys. Geosyst.* **2010**, *11*, Q07006. [CrossRef]
18. Prevosti, M.; Casas, L.; Pérez, J.F.R.; Fouzai, B.; Álvarez, A.; Pitarch, À. Archaeological and Archaeomagnetic Dating at a Site from the Ager Tarraconensis (Tarragona, Spain): El Vila-Sec Roman Pottery. *J. Archaeol. Sci.* **2013**, *40*, 2686–2701. [CrossRef]
19. Casas, L.; Ramírez, J.; Navarro, A.; Fouzai, B.; Estop, E.; Rosell, J.R. Archaeometric Dating of Two Limekilns in an Industrial Heritage Site in Calders (Catalonia, NE Spain). *J. Cult. Herit.* **2014**, *15*, 550–556. [CrossRef]

20. Casas, L.; Prevosti, M.; Fouzai, B.; Álvarez, A. Archaeomagnetic Study and Dating at Five Sites from Catalonia (NE Spain). *J. Archaeol. Sci.* **2014**, *41*, 856–867. [CrossRef]
21. Day, R.; Fuller, M.; Schmidt, V.A. Hysteresis Properties of Titanomagnetites: Grain-Size and Compositional Dependence. *Phys. Earth Planet. Inter.* **1977**, *13*, 260–267. [CrossRef]
22. Paterson, G.A.; Biggin, A.J.; Yamamoto, Y.; Pan, Y. Towards the Robust Selection of Thellier-Type Paleointensity Data: The Influence of Experimental Noise. *Geochem. Geophys. Geosyst.* **2012**, *13*, Q05Z43. [CrossRef]
23. Arrott, A.; Noakes, J.E. Approximate Equation of State for Nickel Near Its Critical Temperature. *Phys. Rev. Lett.* **1967**, *19*, 786–789. [CrossRef]
24. Kono, M.; Tanaka, H. Analysis of the Thelliers' Method of Paleointensity Determination 2. *J. Geomagn. Geoelectr.* **1984**, *36*, 285–297. [CrossRef]
25. Koh, J.; Hogue, J.A.; Wang, Y.; DiSalvo, M.; Allbritton, N.L.; Shi, Y.; Olson, J.A.J.; Sosa, J.A. Single-Cell Functional Analysis of Parathyroid Adenomas Reveals Distinct Classes of Calcium Sensing Behaviour in Primary Hyperparathyroidism. *J. Cell Mol. Med.* **2016**, *20*, 351–359. [CrossRef]
26. Giraldo, J.; Vivas, N.M.; Vila, E.; Badia, A. Assessing the (a)Symmetry of Concentration-Effect Curves: Empirical versus Mechanistic Models. *Pharmacol. Ther.* **2002**, *95*, 21–45. [CrossRef]
27. Benenke, T.W.; Schwippert, W.W. *Datenanalyse Und Präsentation Mit Origin: Anwendungsbeispiele Und Lösungsvorschläge Aus Der Praxis*; Addison-Wesley-Longman: Bonn, Germany, 1997; ISBN 382731061X.
28. Salomon, D. *Hermite Interpolation BT—The Computer Graphics Manual*; Salomon, D., Ed.; Springer: London, UK, 2011; pp. 545–575, ISBN 978-0-85729-886-7.
29. Morales, J.; Goguitchaichvili, A.; Alva-Valdivia, L.M.; Urrutia-Fucugauchi, J. Further Details on the Applicability of Thellier Paleointensity Method: The Effect of Magnitude of Laboratory Field. *Comptes Rendus. Géosci.* **2006**, *338*, 507–513. [CrossRef]
30. Cottrell, R.D.; Tarduno, J.A. In Search of High-Fidelity Geomagnetic Paleointensities: A Comparison of Single Plagioclase Crystal and Whole Rock Thellier-Thellier Analyses. *J. Geophys. Res. Solid Earth* **2000**, *105*, 23579–23594. [CrossRef]
31. Le Goff, M.; Gallet, Y. A New Three-Axis Vibrating Sample Magnetometer for Continuous High-Temperature Magnetization Measurements: Applications to Paleo- and Archeo-Intensity Determinations. *Earth Planet. Sci. Lett.* **2004**, *229*, 31–43. [CrossRef]
32. Gallet, Y.; Le Goff, M. High-Temperature Archeointensity Measurements from Mesopotamia. *Earth Planet. Sci. Lett.* **2006**, *241*, 159–173. [CrossRef]
33. Paterson, G.A.; Tauxe, L.; Biggin, A.J.; Shaar, R.; Jonestrask, L.C. On Improving the Selection of Thellier-Type Paleointensity Data. *Geochem. Geophys. Geosyst.* **2014**, *15*, 1180–1192. [CrossRef]
34. Biggin, A.J.; Perrin, M.; Shaw, J. A Comparison of a Quasi-Perpendicular Method of Absolute Palaeointensity Determination with Other Thermal and Microwave Techniques. *Earth Planet. Sci. Lett.* **2007**, *257*, 564–581. [CrossRef]
35. Biggin, A.J.; Perrin, M.; Dekkers, M.J. A Reliable Absolute Palaeointensity Determination Obtained from a Non-Ideal Recorder. *Earth Planet. Sci. Lett.* **2007**, *257*, 545–563. [CrossRef]
36. Carvallo, C.; Roberts, A.P.; Leonhardt, R.; Laj, C.; Kissel, C.; Perrin, M.; Camps, P. Increasing the Efficiency of Paleointensity Analyses by Selection of Samples Using First-Order Reversal Curve Diagrams. *J. Geophys. Res. Solid Earth* **2006**, *111*, B12103. [CrossRef]